Available online at www.sciencedirect.com
SCIENCE DIRECT®
Journal of Biotechnology 122 (2006) 16–27
Journal of BIOTECHNOLOGY
www.elsevier.com/locate/jbiotec

Effect of mixing on reaction–diffusion kinetics for protein hydrogel-based microchips

D.A. Zubtsov, S.M. Ivanov, A.Yu. Rubina, E.I. Dementieva *, V.R. Chechetkin, A.S. Zasedatelev

Engelhardt Institute of Molecular Biology of Russian Academy of Sciences, Vavilova Str. 32, Moscow 119991, Russia

Received 29 March 2005; received in revised form 11 July 2005; accepted 4 August 2005

Abstract

Protein hydrogel-based microchips are being developed for high-throughput evaluation of the concentrations and activities of various proteins. To shorten the time of analysis, the reaction–diffusion kinetics on gel microchips should be accelerated. Here we present the results of the experimental and theoretical analysis of the reaction–diffusion kinetics enforced by mixing with peristaltic pump. The experiments were carried out on gel-based protein microchips with immobilized antibodies under the conditions utilized for on-chip immunoassay. The dependence of fluorescence signals at saturation and corresponding saturation times on the concentrations of immobilized antibodies and antigen in solution proved to be in good agreement with theoretical predictions. It is shown that the enhancement of transport with peristaltic pump results in more than five-fold acceleration of binding kinetics. Our results suggest useful criteria for the optimal conditions for assays on gel microchips to balance high sensitivity and rapid fluorescence saturation kinetics.

Keywords: Protein hydrogel microchips; Reaction–diffusion kinetics; Peristaltic pump; Antibody–antigen interaction; Fluorescence measurement

1. Introduction

Biological microchips, or arrays of individual elements containing various probes (DNA, proteins, oligosaccharides, cells, etc.), serve as miniature tools for different research and practical purposes (for review see, e.g. Nature Genetics, 2002; Kolchinsky and Mirzabekov, 2002; Cutler, 2003; Seong and Choi, 2003; Stoll et al., 2004). Recently, three-dimensional hydrogel-based microchips with immobilized DNA and proteins were developed at the Moscow Institute of Molecular Biology (Rubina et al., 2003, 2004). Immobilization of probes within three-dimensional hydrogels offers many advantages over two-dimensional surface immobilization used by most microchip manufacturers. In particular, the increase in immobilization

* Corresponding author. Tel.: +7 095 135 99 80; fax: +7 095 135 14 05.
E-mail address: kdem@biochip.ru (E.I. Dementieva).

0168-1656/$ – see front matter © 2005 Elsevier B.V. All rights reserved.
doi:10.1016/j.jbiotec.2005.08.010

Nomenclature

$[Ab_i]$	concentration of immobilized antibodies
$[Ag]_{sol}$	concentration of antigens in solution
D	diffusion coefficient
J_s	signal at saturation
K_{ass}	thermodynamic association constant
R	radius of semispherical gel pad
$\dot{V}$	volume flow rate generated by peristaltic pump
τ_B	saturation (or binding) time

capacity as compared with surface microchips, aqueous surrounding of immobilized compounds, absence of contacts with hydrophobic surface, and stabilizing effect of the gel appear to be especially important for proteins. Gel-based protein microchips were used for studies of protein–protein and protein–ligand interactions for enzymatic reactions and various immunoassays (Rubina et al., 2003; Dementieva et al., 2004; Rubina et al., 2005). The most important applications involve quantitative immunoassay of tumor-associated markers and biological toxins with the sensitivity comparable to or higher than that of standard immunological methods.

As a means of analysis, protein microchips should satisfy two conditions: (i) be sensitive enough to detect low concentrations of ligands or antigens and (ii) the time of analysis should be as short as possible. For gel protein microchips, the time needed for the saturation of observable fluorescence signals is mainly determined by hindered diffusion of antigens into the gel pads and their interaction with the immobilized antibodies. Although diffusion of proteins in different gels has been investigated rather intensively (Williams et al., 1998; Pluen et al., 1999; Ramanujan et al., 2002, and references therein), the study of protein kinetics combining both diffusion and molecular interactions within gel pads has been performed to a much lesser extent. However, for the latter problem we may relate to the previous results of the theoretical and experimental analysis of hybridization kinetics on the oligonucleotide microchips (Livshits and Mirzabekov, 1996; Sorokin et al., 2003; Bhanot et al., 2003; Dorris et al., 2003; Gadgil et al., 2004). The similarity should also be noted between this problem and the classical chemical engineering problem of transport to and into a catalyst particle. Among the extensive literature devoted to the reaction–diffusion kinetics, we may mention (Bird et al., 1960; Moelwyn-Hughes, 1971; Probstein, 1994; Schmidt, 1997; Froment, 2001).

The former investigations have shown that the characteristic hybridization time for the reaction–diffusion kinetics on the oligonucleotide microchips is about 10–20 h (and, as will be shown below, such assessment holds for the protein microchips as well). Therefore, the acceleration of saturation kinetics is highly desirable. Since we are interested primarily in mass application of protein microchip technology, we chose peristaltic pump as standard and inexpensive equipment for the acceleration of kinetics. Among other methods to accelerate the rate of kinetics it is worth mentioning the application of electric field (Heaton et al., 2001; Oddy et al., 2001), acoustic waves (Toegl et al., 2003), and microfluidic devices with different types of mixing (Adey et al., 2002; Yuen et al., 2003; McQuain et al., 2004).

The goal of this work was to compare the reaction–diffusion kinetics on protein hydrogel microchips and its acceleration by mixing buffer solution with peristaltic pump. The experiments were carried out on microchips with immobilized antibodies under the conditions utilized for on-chip immunoassay. To design and interpret the experiments, we present the relevant theory and demonstrate a good agreement between the theoretical predictions and experimental observations. It is shown that the same factors that enhance the final fluorescence intensities result in longer time needed to reach equilibrium and saturation of fluorescence signals. Thus, our results provide useful criteria for the choice of parameters of gel microchips and reaction conditions, which balance high sensitivity and rapid fluorescence saturation kinetics.

2. Materials and methods

Insulin and monoclonal antibodies to insulin were purchased from Sigma (St. Louis, MO, USA); Cy3 fluorescence dye, monosuccinimide ester, Sephadex G-25 coarse, from Amersham Pharmacia Biosciences (Piscataway, NJ, USA); Micro Bio-Spin chromatography columns from Bio-Rad Laboratories (Hercules, CA, USA); glass slides for the fabrication of microar-

rays (Corning 2947 Micro Slides) from Corning Glass Works (Corning, NY, USA). Insulin was labeled with Cy3 according to manufacturer's instructions. Other reagents were obtained from commercial suppliers and used without further purification.

2.1. Manufacturing of microchips

Microchips with immobilized proteins were fabricated by polymerization-mediated immobilization method as described elsewhere (Mirzabekov et al., 2001; Rubina et al., 2003, 2004). Solutions for microchip preparation containing gel components and monoclonal antibodies to insulin (0.12–2 mg/ml) were transferred to the wells of a 384-well microtitration plate (Genetix, New Milton, UK) and spotted onto Bind Silane-treated glass slides using QArray (Genetix, UK) pin robot. Polymerization of gel arrays was carried out under UV light with a maximal wavelength of 350 nm, irradiation intensity 0.06 $\mu W/cm^2$ (GTE lamp F15T8/350 BL, Sylvania, Danvers, MA, USA), for 40 min at 20 °C. Microchips were washed in 0.01 M Na–phosphate, 0.15 M NaCl buffer, pH 7.2 (PBS) containing 0.1% Tween-20. After polymerization and washing, gel elements were 250 μm in diameter, 4 nl in volume, and the distance between the centers of gel elements was 550 μm.

2.2. Fluorescence measurements

Quantitative fluorescence measurements were carried out with a custom-built fluorescence microscope equipped with a cooled CCD-camera, Peltier thermotable, temperature controller, and a computer with data-acquisition board (Barsky et al., 2002). The signals from Cy3 dye were obtained using 535/590 nm excitation/emission filters. Fluorescence signals from individual gel elements were processed using ImaGel Research program developed in our laboratory. All measurements were performed at 25 °C.

The fluorescence signal was defined according to the formula

$$J(t) = \frac{C(t) - C(0)}{B_{\text{r.g.}} - B_{\text{d.c.}}} \quad (1)$$

where $C(t)$ is the integral fluorescence at moment t calculated for the image area occupied by a gel pad, while $C(0)$ the counterpart fluorescence at the initial moment $t = 0$. To take into account possible spatial inhomogeneity of illumination source, the microchip slide was replaced by the slide of red glass of identical sizes and the corresponding integral fluorescence intensity within a position occupied by a gel pad, $B_{\text{r.g.}}$, was measured. This value was corrected by the noise signal $B_{\text{d.c.}}$ produced by dark current at zero illumination intensity.

2.3. On-chip kinetic measurements

Kinetic measurements were carried out with microchips containing immobilized antibodies against insulin in different concentrations and empty gel elements (Fig. 1). The experimental conditions were similar to direct immunoassay of compounds on microchips with immobilized antibodies against insulin (Dementieva et al., 2004; Rubina et al., 2005). Microchips were washed with PBS containing 0.1% Tween-20 (PBST) and water. Insulin-Cy3 was diluted with PBS containing 0.15% polyvinyl alcohol and 0.15% polyvinyl pyrrolidone. To measure the evolution of fluorescence on the chip, a special reaction chamber was constructed (Fig. 2). The chamber was made of quartz glass (cross-section area with respect to the direction of flow generated by peristaltic pump 8 mm × 0.3 mm and length 30 mm) with tubing connectors 0.4 mm in diameter for the supply of reaction liquid inside the chamber. The chamber was fixed on a chip by silicon spacers. The microchip covered with a chamber was mounted on a thermotable. The reaction mixture containing Cy3-labeled insulin (total volume 225 μl) was injected into the chamber through the tubing connectors using micropipette. The volume of the reaction chamber was 75 μl, while the remaining 150 μl were distributed between the two tubing connectors. If the experiment was carried out without mixing, the connectors were sealed or joined with each other. Fluorescence signals from each gel element were measured every 60 s for 6–20 h at different concentrations of the antigen in buffer solution, and the results were processed as described above. To control the variations in the readings, each antibody concentration was represented by four identical gel pads (Fig. 1), and the fluorescence signals were calculated by the median value for the set of four pads. Additionally, we used a set without immobilized antibodies to assess the background signals.

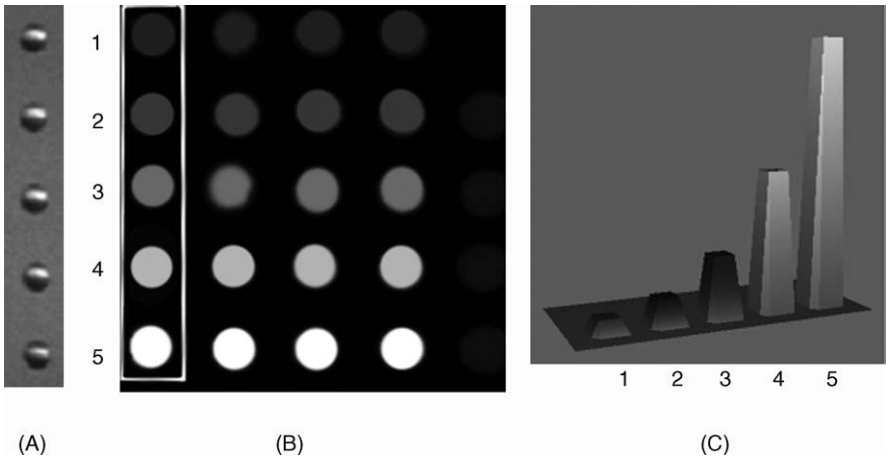

Fig. 1. Gel-based protein microchip used for this study. (A) Photograph of microchip gel elements in transmitted light. (B) Microchip containing immobilized antibodies to insulin after the binding with Cy3-labeled insulin. Concentrations of antibodies were 0.04 (horizontal row 1, four elements), 0.08 (horizontal row 2, four elements), 0.15 (horizontal row 3, four elements), 0.3 (horizontal row 4, four elements), and 0.6 (horizontal row 5, four elements) mg per ml of gel. Four elements in the right vertical row contain no antibodies and are nearly invisible. (C) Three-dimensional fluorescence images of gel elements with different concentration of immobilized antibodies obtained using ImaGel Research software.

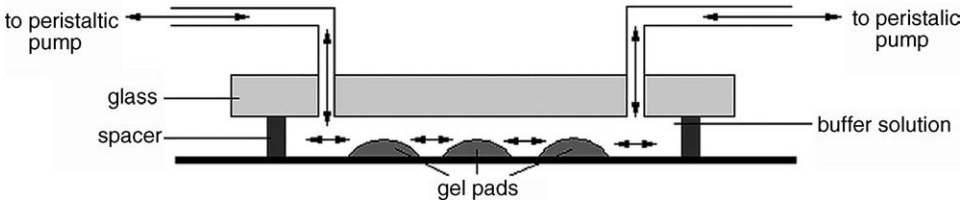

Fig. 2. Scheme of the chamber with inlet/outlet ports for the injection of reaction liquid inside the chamber and mixing with peristaltic pump.

To generate a mixing flow in the reaction chamber, the inlet/outlet ports were joined with a Minipulse 2 (Gilson, France) peristaltic pump, which was modified to function in oscillation mode. Insulin-Cy3 solution was pumped through the chamber. Mixing was achieved by switching the flow direction from direct to reverse every 2 s; the standard volume flow rate was 6 ml/min. By adding the dye into one of the tubing connector, we found that homogeneous mixing in the chamber is achieved at this rate in about 2 min.

The association constant K_{ass} for the reaction of immobilized antibody–insulin complex formation was determined by the two methods: (i) from the dependence of saturation fluorescence signals on insulin concentration (see Eq. (3) below) obtained upon the binding of insulin-Cy3 with on-chip-immobilized antibodies; (ii) as a ratio of association and dissociation rates k_{ass}/k_{diss} obtained using a BIAcore instrument (Pharmacia Biosensor AB, Uppsala, Sweden) with the same monoclonal antibodies as an immobilized sensor and insulin-Cy3 in solution.

The experiments were completed on a batch of 60 identical protein microchips as described above. All experiments at a given concentration of antigen in solution and with or without mixing were repeated twice. The lowest signal-to-noise ratio exceeded 2.5, while the relative scattering in experimental data was within 5–10%.

3. Results

3.1. General overview

Our aims are to determine the main factors influencing the saturation kinetics on the gel protein microchips

and to choose optimal concentrations of the immobilized antibodies and analyzed antigens. The use of microchips enables us to perform parallel measurements at different concentrations of immobilized antibodies. In particular, we used the scheme of microchip shown in Fig. 1, where the concentrations of the immobilized antibodies to insulin were consecutively doubled in the sets of oblate semispherical gel pads starting from the lowest concentration $[Ab_i] = 0.04$ mg/ml (or 2.6×10^{-7} M) up to the grade of $2^4 \times [Ab_i]$.

Throughout our experiments the antigens were invariably in excess in the sense of inequality

$$V_{pad}[Ab_i] \ll V_{chamber}[Ag]_{sol} \quad (2)$$

where V_{pad} and $V_{chamber}$ are respectively the volumes of a separate gel pad and of the chamber, $[Ab_i]$ the concentration of immobilized antibodies, and $[Ag]_{sol}$ the concentration of antigens in buffer solution. The inequality Eq. (2) was always fulfilled by more than two orders of magnitude. Therefore, the depletion of antigens in buffer solution during their binding with antibodies may be neglected.

The resulting saturation signal for the reaction–diffusion kinetics $J_{s,diff}$ is attained at the thermodynamic equilibrium and is proportional to the equilibrium concentration of antibody–antigen complexes $[C]_{eq}$ (see also Appendix A)

$$J_{s,diff} = A[C]_{eq} = A[Ab_i]\frac{K_{ass}[Ag]_{sol}}{1 + K_{ass}[Ag]_{sol}} \quad (3)$$

Here A is the apparatus constant and K_{ass} the thermodynamic association constant. The corresponding saturation times for reaction–diffusion kinetics were experimentally assessed from the kinetic curves via the time needed to attain 0.9 level from signal at saturation and may be approximated as (cf. Sorokin et al., 2003; see also Appendix A).

$$\tau_{B,diff} = \tau_D \varphi(D_{gel}/D_{sol}; K_{ass}[Ag]_{sol})[Ab_i] \times \frac{K_{ass}}{1 + K_{ass}[Ag]_{sol}} \quad (4)$$

where the diffusion time $\tau_D \cong R^2/D_{gel}$ corresponds to the diffusion of antigens in a gel pad with radius R containing no immobilized antibodies, D_{gel} is the corresponding diffusion coefficient, while D_{sol} the diffusion coefficient for a buffer solution, and the factor φ is of the order of unity and weakly decreases with the increase of $K_{ass}[Ag]_{sol}$. For simplicity, the factor φ was attributed to τ_D in fitting the experimental data (i.e. it was taken $\varphi = 1$).

The relevant theory for the on-chip kinetics forced by peristaltic pump is yet absent. Some essential features related to the hydrodynamic flow in the chamber and its penetration into the gel pads are briefly discussed in Appendix A. One of the main results of this work is that the complicated kinetics under these conditions may be presented in a rather simple form analogous to Eq. (4).

3.2. Kinetic curves, signals at saturation and saturation times. Comparison of two kinetic regimes and comparison of theory with experiments

In this section, we compare the characteristics of two kinetic regimes and our experimental results with theoretical predictions. The primary information is obtained from the kinetic saturation curves like those shown in Fig. 3, which reflect the antigen binding at different concentration of immobilized antibodies and concentration of insulin 100 ng/ml. Similar curves were obtained for other concentrations of antigen within the 30–1000 ng/ml (4.8–160 nM) range. All the data for the kinetics forced by peristaltic pump are referred to the volume flow rate $\dot{V} = 6$ ml/min. The level of saturation for signals in our experiments was defined by the criterion that the observable changes in signals were not registered for 3 h in the diffusion regime and for 1 h in the case of kinetics with peristaltic pump. The control experiments with extended lapse of time showed the applicability of this criterion.

The dependence of signals at saturation on the concentration of immobilized antibodies $[Ab_i]$ appears to be linear in both kinetic regimes (Fig. 4). Since the saturation signals for the reaction–diffusion kinetics are determined by thermodynamic Eq. (3), their dependence on the concentration of antigen in solution $[Ag]_{sol}$ allows us to determine thermodynamic association constant K_{ass}. The corresponding fitted value $K_{ass} = (4.5 \pm 0.4) \times 10^7\ M^{-1}$ turned out to be in a very good agreement with the association constant measured by a completely different BIAcore technique, which employs surface plasmon resonance phenomenon. Because the concentration of antigens appears in all expressions in the form of product

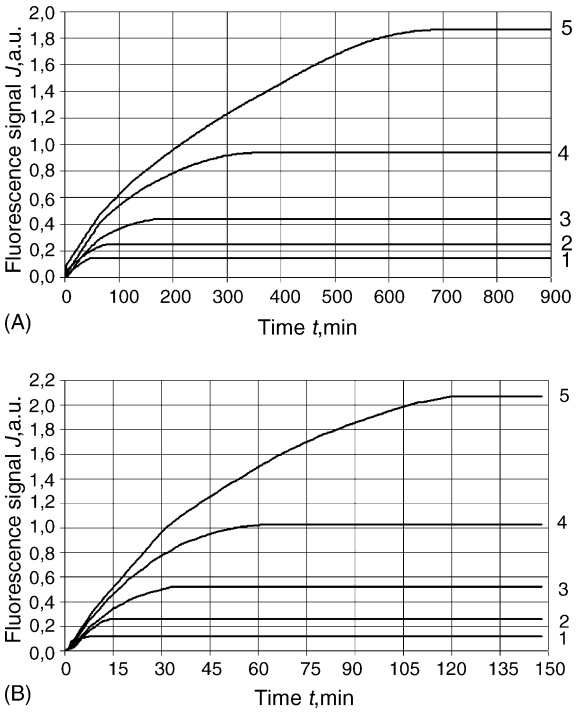

Fig. 3. Kinetic curves for (A) diffusion–reaction kinetics and (B) kinetics forced by peristaltic pump at concentration of antigen in solution $[Ag]_{sol} = 100$ ng/ml and different concentrations of immobilized antibodies in the gel pads. Numerals along the right edge of the graph indicate concentrations of immobilized antibodies as described in Fig. 1.

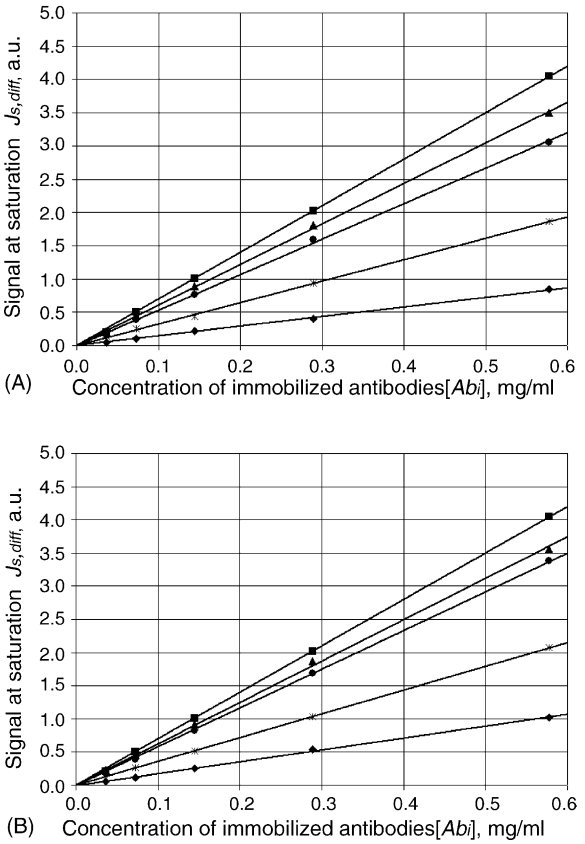

Fig. 4. Dependence of signals at saturation on the concentration of immobilized antibodies for (A) diffusion–reaction kinetics and (B) kinetics forced by peristaltic pump. Concentrations of antigen in solution $[Ag]_{sol}$ are 30 (♦); 100 (✕); 300 (●); 500 (▲); and 1000 (■) ng/ml. The lines correspond to the best linear fit of experimental data.

$K_{ass}[Ag]_{sol}$, the corresponding dependence of saturation signals and saturation times will be given as a function of the product $K_{ass}[Ag]_{sol}$, instead of specific concentration $[Ag]_{sol}$. As expected, the dependence of saturation signals on the antigen concentration is well described by thermodynamic Eq. (3) in the case of reaction–diffusion kinetics (see Fig. 5(A)), while the deviations from thermodynamic equilibrium turned out rather small for the kinetics forced by peristaltic pump (cf. Fig. 5(B) and (C)).

The saturation (or binding) time τ_B was determined from the kinetic curves when the fluorescence signal reached 0.9 of the saturation level. Again, the dependence of saturation time on the concentration of immobilized antibodies is linear in both regimes (Fig. 6). The corresponding dependence of τ_B on the antigen concentration supports the theoretical prediction given by Eq. (4) for the case of reaction–diffusion kinetics and provides $\tau_D = 5.4 \pm 0.2$ min (see Fig. 7(A)). At the radius of the semispherical gel pads $R \sim 10^{-2}$ cm, such a diffusion time τ_D provides an estimate for the diffusion coefficient in the gel $D_{gel} \sim 5 \times 10^{-7}$ cm^2/s, which is similar to typical values for the diffusion of proteins in different gels (cf. Williams et al., 1998; Pluen et al., 1999; Ramanujan et al., 2002). We found that the corresponding saturation times for the kinetics forced by peristaltic pump may well be described by the dependence

$$\tau_{B,pump} = \tau_P[Ab_i]\frac{K_{ass}}{1 + K_{ass}[Ag]_{eff}} \quad (5)$$

where time τ_P is the fitting parameter and the concentrations of antigens $[Ag]_{eff}$ shifted from thermody-

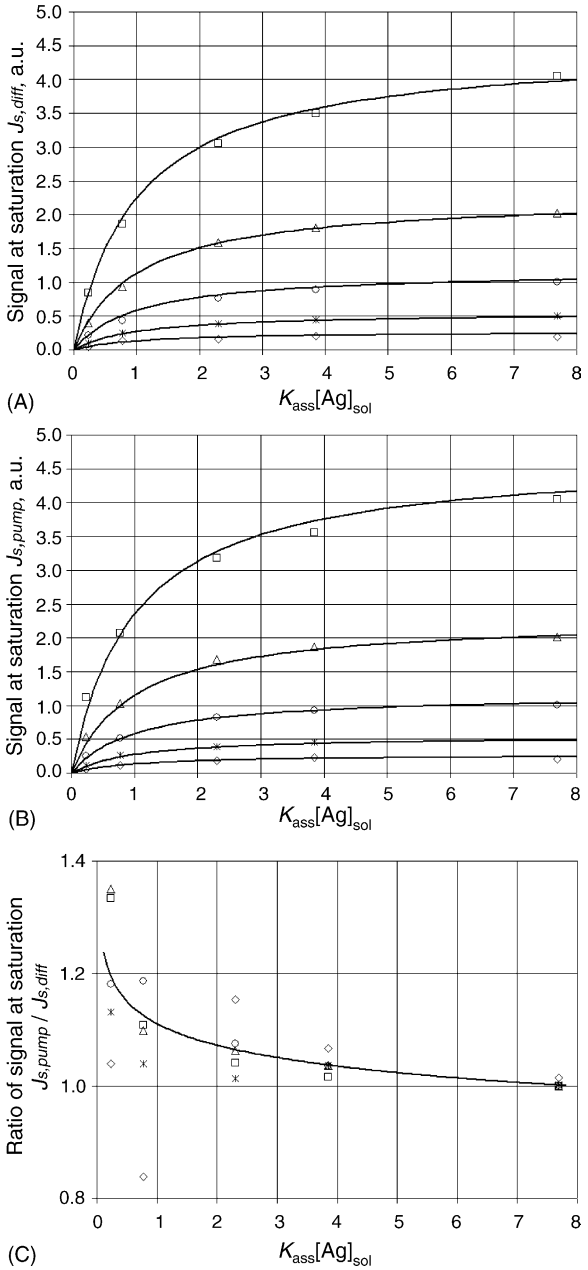

Fig. 5. Dependence of signals at saturation on the concentration of insulin in solution. (A) Diffusion–reaction kinetics. The curves correspond to prediction defined by Eq. (3) with the association constant $K_{ass} = 4.5 \times 10^7\ M^{-1}$. (B) Kinetics forced by peristaltic pump. (C) Ratio of signals at saturation for the two kinetic regimes. The spline curve is drawn through the points averaged over concentrations of immobilized antibodies. Concentrations of immobilized antibodies $[Ab_i]$ are 0.04 (◊); 0.08 (✕); 0.15 (○); 0.3 (△); and 0.6 (□) mg/ml.

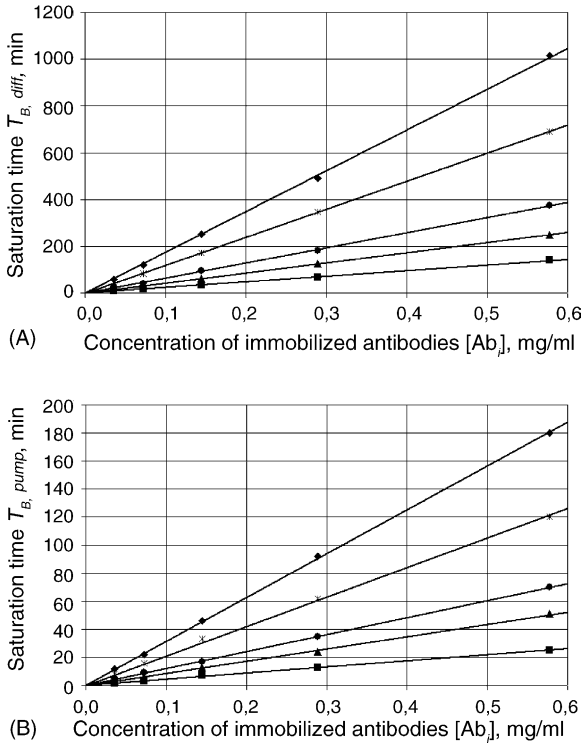

Fig. 6. Dependence of the saturation time on the concentration of immobilized antibodies for (A) diffusion–reaction kinetics and (B) kinetics forced by peristaltic pump. Concentrations of antigen in solution $[Ag]_{sol}$ are 30 (♦); 100 (✕); 300 (●); 500 (▲); and 1000 (■) ng/ml. The lines correspond to the best linear fit of experimental data.

namic equilibrium are calculated via signals at saturation according to

$$J_{s,pump} = A[Ab_i]\frac{K_{ass}[Ag]_{eff}}{1 + K_{ass}[Ag]_{eff}} \quad (6)$$

while all other parameters in Eq. (5) are assumed to be known either from the chip manufacturing or from reaction–diffusion kinetics. As is seen from Fig. 7(B), the experimental dependence is well fitted by Eq. (5) with time $\tau_P \cong 1.1 \pm 0.1$ min.

3.3. Dependence of signals at saturation and saturation times on flow rate

Additional information about the mechanisms of acceleration in reaction–diffusion kinetics may be

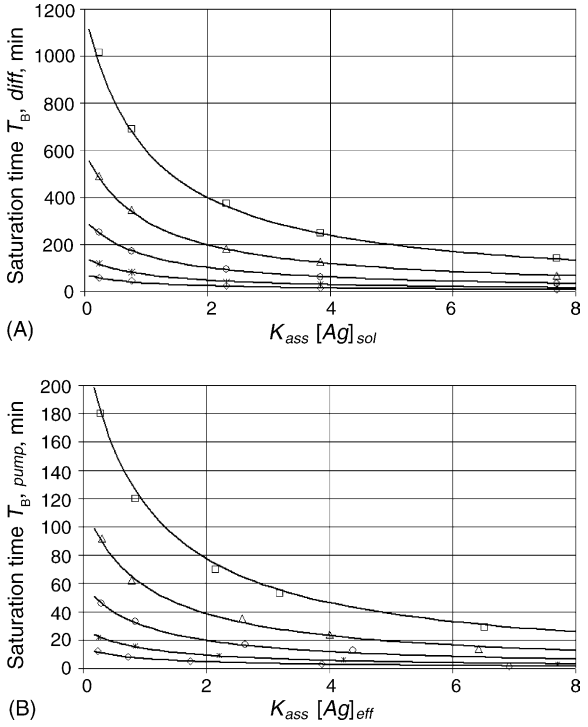

Fig. 7. Dependence of the saturation time on the concentration of antigen in solution. (A) Diffusion–reaction kinetics. Solid curves correspond to the theoretically predicted function defined by Eq. (4) with fitted diffusion time τ_D. (B) Kinetics forced by peristaltic pump. Solid curves are fitted with Eq. (5). Concentrations of immobilized antibodies [Ab$_i$] are 0.04 (◊); 0.08 (✖); 0.15 (◯); 0.3 (△); and 0.6 (□) mg/ml.

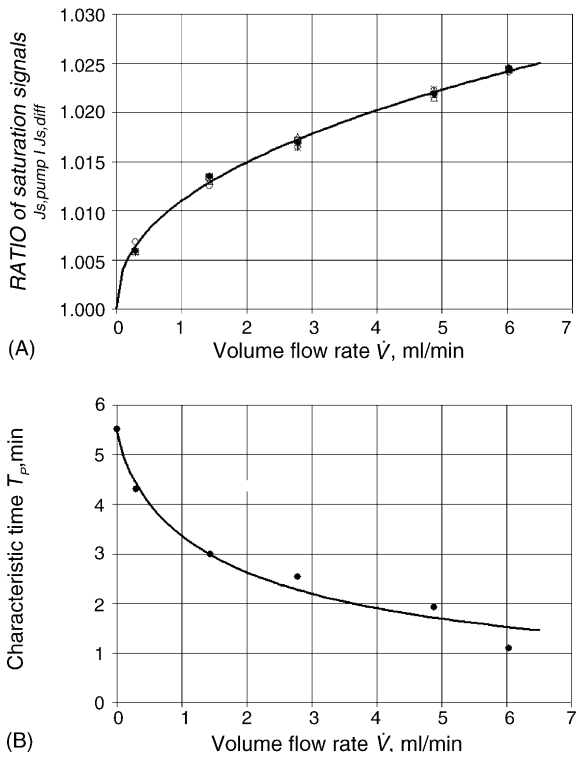

Fig. 8. (A) Dependence of ratio of signals at saturation $J_{s,pump}/J_{s,diff}$ on the flow rate $\dot{V}$ generated by peristaltic pump. Concentrations of immobilized antibodies [Ab$_i$] are 0.04 (◊); 0.08 (✖); 0.15 (◯); 0.3 (△); and 0.6 (□) mg/ml. Solid curve is fitted with Eq. (7). (B) Dependence of mean characteristic time τ_P (see Eq. (5)) on the flow rate $\dot{V}$. Solid curve is fitted with Eq. (8). Both in (A) and (B) the concentration of antigen in solution [Ag]$_{sol}$ is 500 ng/ml.

obtained by studying dependencies of different characteristics on the flow rate $\dot{V}$. Fig. 8(A) shows the dependence of ratio of saturation signals $J_{s,pump}/J_{s,diff}$ on the flow rate generated by peristaltic pump at the concentration of antigen in solution [Ag]$_{sol}$ = 500 ng/ml. The experimental dependence is compared with approximation

$$\frac{J_{s,pump}}{J_{s,diff}} = 1 + a_J \dot{V}^{b_J} \quad (7)$$

where a_J and b_J are fitting parameters. The best fitting provides the values $a_J = 0.011$ and $b_J = 0.44$ (note that, unlike index b_J, parameter a_J is dimensional and implies that $\dot{V}$ is measured in ml/min). The characteristic time τ_P (see Eq. (5) and Fig. 8(B)) was recalculated from the observable saturation times and averaged over concentrations of immobilized antibodies. The fitting with approximation

$$\tau_P = \frac{\tau_D}{1 + a_\tau \dot{V}^{b_\tau}} \quad (8)$$

yields the parameters $a_\tau = 0.62$ and $b_\tau = 0.79$. Here the diffusion time τ_D is the same as in Eq. (4).

The fitted index b_J turned out rather close to 0.5 and indicates the effects related to the hydrodynamic and diffusion boundary layers around semispherical gel pad (Probstein, 1994), while index b_τ is close to 1.0 and is compatible with both external transport effects and Darcy–Brinkman penetration into the gel (see Appendix A).

4. Discussion

Our results demonstrate that the mixing with peristaltic pump provides about five-fold acceleration in reaction–diffusion kinetics for protein gel microchips. First of all, peristaltic pump accelerates the external transport of antigens to the gel pads. To assess these effects and avoid rather complicated numerical solution of Navier–Stokes equation, we performed the simplified simulation of reaction–diffusion kinetics with variable diffusion ratio D_{gel}/D_{sol} and zero flow rate $\boldsymbol{u}$. The simulations with the program ImaGel 3D Kinetics of the reaction–diffusion kinetics corresponding to Eqs. (A.1)–(A.5) in the Appendix A (where $\boldsymbol{u} = 0$) show that the diminishing of ratio D_{gel}/D_{sol} in Eq. (4) from 0.2 to zero (the latter value emulates the enhancement of transport by peristaltic pump) causes the decrease in factor φ by 2–2.5 times. Thus, though the effect of external transport is significant, it is likely that there are also other factors in kinetics acceleration.

These additional factors may be related to the partial penetration of antigens into the gel pads via Darcy–Brinkman leakage. The estimates in the Appendix A indicate that such a mechanism might compete with diffusion within the pads if the hydrodynamic screening is incomplete.

Under our conditions, the hydrodynamic pressure on the gel pads $\rho(\dot{V}/S)^2$ was about ~10 dyne/cm^2, and the contribution of viscous forces to the stress tensor was approximately the same. Such oscillating pressure may cause dynamic deformations of gel network and also increase the diffusion within the pad (De Gennes, 1979). These effects are, however, difficult to assess.

The analysis shows (see Eqs. (3)–(5)) that such factors as the association constant K_{ass} and the concentration of the immobilized antibodies $[Ab_i]$ influence both the equilibrium fluorescence intensity and the binding time needed to attain saturation level. The higher the concentration of immobilized antibodies and the higher the association constant, the higher the concentration of the formed complexes and the stronger the corresponding fluorescence signal, but, simultaneously, the longer the time needed to reach equilibrium. Thus, the optimal choice of these parameters depends on the required fluorescence intensity and reasonable binding time. The application of mixing may significantly speed up binding kinetics preserving or even enhancing the strength of signals at saturation (cf. Figs. 5 and 7). The relative enhancement of signals is, however, sufficiently less than the enhancement reported previously for surface oligonucleotide microchips (Adey et al., 2002; Toegl et al., 2003; McQuain et al., 2004). The difference may partially be due to the fact that in the latter experiments the enhancement of signals has been measured in the transient regimes far from saturation level.

Although the expression for saturation time like that given by Eq. (5) was proved for mixing with peristaltic pump, it may be applicable for the other mechanisms of mixing as well. The particular mode of mixing should affect mainly the characteristic time τ_P, while the second factor in Eq. (5) depends on the general kinetic balance and local equilibrium within separate gel pad (cf. Appendix A).

We conclude that mixing with peristaltic pump results in about five-fold acceleration in reaction–diffusion kinetics for the hydrogel-based protein microchips. Surely, the application of some kind of mixing will be necessary for further development of efficient microchip technologies.

Acknowledgements

The authors thank E.Ya. Kreindlin, K.B. Yevseyev, O.G. Somova, O.V. Moiseeva, and E.N. Savvateeva for microchip manufacturing, V.V. Petukhov and A.A. Stomakhin for the construction of mixing device, N.V. Sorokin, M.A. Livshits, and A.Yu. Turygin for useful discussions and help in this work. We are especially grateful to A.M. Kolchinsky, Health Front Line, Ltd. (Champaign, IL) for his assistance in the manuscript preparation. This work was supported by CRDF Project # RUC2–11036-MO-04 and ISTC Project #3117.

Appendix A

A.1. Reaction–diffusion kinetics and saturation time

For the convenience of the reader, we derive in this Appendix the expression for saturation time in the case of diffusion–reaction kinetics (Eq. (4)). Here our consideration will mainly be qualitative (the more detailed theory for diffusion kinetics can be found in Sorokin et al., 2003). The transport of antigen in the solution

outside the region of gel pad is defined as

$$\frac{\partial[\mathrm{Ag}]}{\partial t} + (\boldsymbol{u}\cdot\nabla)[\mathrm{Ag}] = D_{\mathrm{sol}}\nabla^2[\mathrm{Ag}] \tag{A.1}$$

where [Ag] corresponds to the local concentration of antigen in solution, D_{sol} is diffusion coefficient for the antigen diffusing in solution, and $\boldsymbol{u}$ the velocity of solution generated by peristaltic pump. If the penetration of flow inside gel pad may neglected (see below), then the resulting reaction–diffusion kinetics within a gel pad is given by

$$\frac{\partial[\mathrm{Ag}]}{\partial t} = D_{\mathrm{gel}}\nabla^2[\mathrm{Ag}] - k_{\mathrm{ass}}([\mathrm{Ab_i}] - [C])\,[\mathrm{Ag}] + k_{\mathrm{diss}}[C] \tag{A.2}$$

$$\frac{\partial[C]}{\partial t} = k_{\mathrm{ass}}([\mathrm{Ab_i}] - [C])\,[\mathrm{Ag}] - k_{\mathrm{diss}}[C] \tag{A.3}$$

Here $[\mathrm{Ab_i}]$ is the concentration of the immobilized antibodies, [Ag] and $[C] = [\mathrm{Ab_i}\cdot\mathrm{Ag}]$ the local concentrations of antigens and antigen–antibody complexes within gel pad, k_{diss} and k_{ass}, respectively, the rates of dissociation and association, and D_{gel} the diffusion coefficient for the antigen diffusing in a gel. At the surface of a gel pad, S_{pad}, the concentration and the normal component of transport flow for antigen should be continuous,

$$[\mathrm{Ag}]^{(\mathrm{sol})}|_{\boldsymbol{r}\in S_{\mathrm{pad}}} = [\mathrm{Ag}]^{(\mathrm{pad})}|_{\boldsymbol{r}\in S_{\mathrm{pad}}} \tag{A.4}$$

$$D_{\mathrm{sol}}\boldsymbol{n}_{\mathrm{S}}\cdot\nabla[\mathrm{Ag}]^{(\mathrm{sol})}|_{\boldsymbol{r}\in S_{\mathrm{pad}}} = D_{\mathrm{gel}}\boldsymbol{n}_{\mathrm{S}}\cdot\nabla[\mathrm{Ag}]^{(\mathrm{pad})}|_{\boldsymbol{r}\in S_{\mathrm{pad}}} \tag{A.5}$$

where $\boldsymbol{n}_{\mathrm{S}}$ is the unit vector normal to the surface of a gel pad and the normal component of velocity $\boldsymbol{u}$ was taken to be zero at the surface.

Due to the conservation law, the evolution for the sum of concentrations of the antigens and complexes within gel pad depends exclusively on the diffusion of antigen

$$\frac{\partial([\mathrm{Ag}] + [C])}{\partial t} = D_{\mathrm{gel}}\nabla^2[\mathrm{Ag}] \tag{A.6}$$

Commonly, the saturation time is long enough and the inequalities $\tau_{\mathrm{B,diff}} \gg k_{\mathrm{diss}}^{-1}, (k_{\mathrm{ass}}[\mathrm{Ab_i}])^{-1}$ are satisfied. Therefore, local concentrations of the complex and antigen may approximately be related by the condition of local thermodynamic equilibrium,

$$[C] \cong [\mathrm{Ab_i}]\frac{K_{\mathrm{ass}}[\mathrm{Ag}]}{1 + K_{\mathrm{ass}}[\mathrm{Ag}]} \tag{A.7}$$

where $K_{\mathrm{ass}} = k_{\mathrm{ass}}/k_{\mathrm{diss}}$ is thermodynamic association constant. Due to the design of the microchip, $K_{\mathrm{ass}}[\mathrm{Ab_i}] \gg 1$ (i.e. gel pads should emit rather strong fluorescence signals and act as effective enhancers of antigen concentration), and the concentration of antigen may be neglected with respect to that of complex in the left part of Eq. (A.6). Then, introducing the dimensionless variables $\tilde{\boldsymbol{r}} = \boldsymbol{r}/R$; $[\tilde{\mathrm{Ag}}] = [\mathrm{Ag}]/[\mathrm{Ag}]_{\mathrm{sol}}$; $[\tilde{C}] = [C]/[C]_{\mathrm{eq}}$, where R is the radius of semispherical gel pad and

$$[C]_{\mathrm{eq}} = [\mathrm{Ab_i}]\frac{K_{\mathrm{ass}}[\mathrm{Ag}]_{\mathrm{sol}}}{1 + K_{\mathrm{ass}}[\mathrm{Ag}]_{\mathrm{sol}}} \tag{A.8}$$

it is easy to see that the dimensionless time would be measured as $\tilde{t} = t/\tau_{\mathrm{B,diff}}$ with $\tau_{\mathrm{B,diff}}$ defined by Eq. (4) (up to the function φ). Note that the characteristic time related to the diffusion of antigen in solution outside gel pad, $\tau_{\mathrm{diff}}^{(\mathrm{sol})} \cong R^2/D_{\mathrm{sol}}$, is commonly several orders of magnitude less than $\tau_{\mathrm{B,diff}}$.

If the hydrodynamic flow would penetrate inside gel, then the diffusion terms in Eqs. (A.2) and (A.6) should be replaced by

$$D_{\mathrm{gel}}\nabla^2[\mathrm{Ag}] \to D_{\mathrm{gel}}\nabla^2[\mathrm{Ag}] - (\boldsymbol{u}\cdot\nabla)\,[\mathrm{Ag}] \tag{A.9}$$

For $D_{\mathrm{gel}} \sim 10^{-7}$ cm^2/s and $R \sim 10^{-2}$ cm, the effects of directed transport become significant if $\boldsymbol{u} \geq D_{\mathrm{gel}}/R \sim 10^{-5}$ cm/s.

A.2. Hydrodynamic flow for transport forced by peristaltic pump and screening effect

The flow generated by peristaltic pump within a chamber is determined by Navier–Stokes and continuity equations

$$\frac{\partial\boldsymbol{u}}{\partial t} + (\boldsymbol{u}\cdot\nabla)\,\boldsymbol{u} = -\frac{1}{\rho}\nabla P + \nu\nabla^2\boldsymbol{u} \tag{A.10}$$

$$\nabla\cdot\boldsymbol{u} = 0 \tag{A.11}$$

with the proper boundary conditions. Here $\boldsymbol{u}$ is the velocity of buffer solution, P the exerted pressure, ρ mass density of buffer solution, and ν kinematic viscosity. The corresponding locally averaged flow in a gel

pad may be described by Brinkman equation (Wiegel, 1980; Sahimi, 1995)

$$\frac{\mu}{\kappa}\boldsymbol{u} = -\nabla P + \mu\nabla^2\boldsymbol{u} \tag{A.12}$$

where κ is the permeability and μ the viscosity of the gel, with the condition of incompressibility given by Eq. (A.8). Combining Eqs. (A.7) and (A.9), it can be deduced that the hydrodynamic flow penetrates into a gel pad at the characteristic distance

$$l_\mathrm{p} \cong \max(\kappa^{1/2}, l) \tag{A.13}$$

$$l \cong \frac{u}{f} \cong \frac{\kappa}{\mu f}|\nabla P| \cong \frac{\kappa}{\mu f}\frac{12\rho\nu(\dot{V}/S)}{h^2} \tag{A.14}$$

Here $\dot{V}$ is the volume flow rate produced by peristaltic pump in the chamber, S and h, respectively, the cross-section area and the height of the chamber, and f the frequency of flow oscillations. In Eq. (A.14), it was assumed that $h^2 f/\nu \ll 1$, which means that viscous forces dominate over inertial effects (plane Poiseuille-like flow). This inequality is fulfilled in our conditions. For $\kappa \sim 10^{-10}$ to $10^{-11}\,\mathrm{cm}^2$, $\mu/\rho \sim 10^{-2}$ to $5\times10^{-2}\,\mathrm{cm}^2/\mathrm{s}$, $\nu \sim 10^{-2}\,\mathrm{cm}^2/\mathrm{s}$, $\dot{V} \sim 5\,\mathrm{ml/min}$, $S \sim 10^{-2}\,\mathrm{cm}^2$, $h \sim 10^{-2}\,\mathrm{cm}$, and $f \sim 1$ cycle/s the penetration length does not exceed $l_\mathrm{p} \sim 0.1$ micron. Note, however, that due to entangled nature of the gel network the expulsion of infiltrated solution from the opposite sides of a gel pad during half-periods of pressure oscillations may be incomplete and the slow creeping infiltration cannot be excluded.

References

Adey, N.B., Lei, M., Howard, M.T., Jensen, J.D., Mayo, D.A., Butel, D.L., Coffin, S.C., Moyer, T.C., Slade, D.E., Spute, M.K., Hancock, A.M., Eisenhoffer, G.T., Dalley, B.K., McNeely, M.R., 2002. Gains in sensitivity with a device that mixes microarray hybridization solution in a 25-micron-thick chamber. Anal. Chem. 74, 6413–6417.

Barsky, V., Perov, A., Tokalov, S., Chudinov, A., Kreindlin, E., Sharonov, A., Kotova, E., Mirzabekov, A., 2002. Fluorescence data analysis on gel-based biochips. J. Biomol. Screening 7, 247–257.

Bhanot, G., Louzoun, Y., Zhu, J., DeLisi, C., 2003. The importance of thermodynamic equilibrium for high throughput gene expression arrays. Biophys. J. 84, 124–135.

Bird, R.B., Stewart, W.E., Lightfoot, E.N., 1960. Transport Phenomena. Wiley, New York.

Cutler, P., 2003. Protein arrays: the current state-of-the-art. Proteomics 3, 3–18.

De Gennes, P.G., 1979. Scaling Concepts in Polymer Physics. Cornell University Press, Ithaca and London.

Dementieva, E.I., Rubina, A.Yu., Darii, E.L., Dyukova, V.I., Zasedatelev, A.S., Osipova, T.V., Ryabykh, T.P., Baryshnikov, A.Yu., Mirzabekov, A.D., 2004. Protein microchips in quantitative assays for tumor markers. Dokl. Biochem. Biophys. 395, 88–92.

Dorris, D.R., Nguen, A., Gieser, L., Lockner, R., Lublinsky, A., Patterson, M., Touma, E., Sendera, T.J., Elghanian, R., Mazumder, A., 2003. Oligodeoxyribonucleotide probe accessibility on a three-dimensional DNA microarray surface and the effect of hybridization time on the accuracy of expression ratios. BMC Biotechnol. 3, 6–16.

Froment, G.F., 2001. Reaction Kinetics and the Development and Operation of Catalytic Processes. Elsevier, Amsterdam and New York.

Gadgil, C., Yeckel, A., Derby, J.J., Hu, W.-S., 2004. A diffusion-reaction model for DNA microarray assays. J. Biotechnol. 114, 31–45.

Heaton, R.J., Peterson, A.V., Georgiadis, R.M., 2001. Electrostatic surface plasmon resonance: direct electric field-induced hybridization and denaturation in monolayer nucleic acid films and label-free discrimination of base mismatches. Proc. Natl. Acad. Sci. U.S.A. 98, 3701–3704.

Kolchinsky, A., Mirzabekov, A.D., 2002. Analysis of SNPs and other genomic variations using gel-based chips. Hum. Mutat. 19, 343–360.

Livshits, M.A., Mirzabekov, A.D., 1996. Theoretical analysis of the kinetics of DNA hybridization with gel-immobilized oligonucleotides. Biophys. J. 71, 2795–2801.

McQuain, M.K., Seale, K., Peek, J., Fisher, T.S., Levy, S., Stremler, M.A., Haselton, F.R., 2004. Chaotic mixer improves microarray hybridization. Anal. Biochem. 325, 215–226.

Mirzabekov, A.D., Rubina, A.Yu., Pan'kov, S.V., 2001. Composition for polymerizing immobilization of biological molecules and method for producing said composition, Russian patent N 2216547; patent PCT/RU 01/00420. Priority 10/16/2001.

Moelwyn-Hughes, E.A., 1971. The Chemical Statics and Kinetics of Solutions. Academic Press, London and New York.

Nature Genetics, Supplement, 2002. The chipping forecast II. 32, 461–552.

Oddy, M.H., Santiago, J.G., Mikkelsen, J.C., 2001. Electrokinetic instability micromixing. Anal. Chem. 73, 5822–5832.

Pluen, A., Netti, P.A., Jain, R.K., Berk, D.A., 1999. Diffusion of macromolecules in agarose gels: comparison of linear and globular configurations. Biophys. J. 77, 542–552.

Probstein, R.F., 1994. Physicochemical Hydrodynamics. Wiley, New York.

Ramanujan, S., Pluen, A., McKee, T.D., Brown, E.B., Boucher, Y., Jain, R.K., 2002. Diffusion and convection in collagen gels: implications for transport in the tumor interstitium. Biophys. J. 83, 1650–1660.

Rubina, A.Yu., Dementieva, E.I., Stomakhin, A.A., Darii, E.L., Pan'kov, S.V., Barsky, V.E., Ivanov, S.M., Konovalova, E.V., Mirzabekov, A.D., 2003. Hydrogel-based protein microchips:

manufacturing, properties, and applications. Biotechniques 34, 1008–1022.

Rubina, A.Yu., Dyukova, V.I., Dementieva, E.I., Stomakhin, A.A., Nesmeyanov, V.A., Grishin, E.V., Zasedatelev, A.S., 2005. Quantitative immunoassay of biotoxins on hydrogel-based protein microchips. Anal. Biochem 340, 317–329.

Rubina, A.Yu., Pan'kov, S.V., Dementieva, E.I., Pen'kov, D.N., Butygin, A.V., Vasiliskov, V.A., Chudinov, A.V., Mikheikin, A.L., Mikhailovich, V.M., Mirzabekov, A.D., 2004. Hydrogel drop microchips with immobilized DNA: properties and methods for large-scale production. Anal. Biochem. 325, 92–106.

Sahimi, M., 1995. Flow and Transport in Porous Media and Fractured Rock. VCH, Weinheim.

Schmidt, L.D., 1997. The Engineering of Chemical Reactions (Topics in Chemical Engineering). Oxford University Press, Oxford.

Seong, S., Choi, C., 2003. Current status of protein chip development in terms of fabrication and application. Proteomics 3, 2176–2189.

Sorokin, N.V., Chechetkin, V.R., Livshits, M.A., Vasiliskov, V.A., Turygin, A.Y., Mirzabekov, A.D., 2003. Kinetics of hybridization on the oligonucleotide microchips with gel pads. J. Biomol. Struct. Dynamics 21, 279–288.

Stoll, D., Bachmann, J., Templin, M.F., Joos, T.O., 2004. Microarray technology: an increasing variety of screening tools for proteomic research. Targets 3, 24–31.

Toegl, A., Kirchner, R., Gauer, C., Wixforth, A., 2003. Enhancing results of microarray hybridization through microagitation. J. Biomol. Techn. 14, 197–204.

Wiegel, W.F., 1980. Fluid Flow Through Porous Macromolecular Systems. Springer-Verlag, Berlin.

Williams Jr., J.C., Mark, L.A., Eichholtz, S., 1998. Partition and permeation of dextran in polyacrylamide gel. Biophys. J. 75, 493–502.

Yuen, P.K., Li, G., Bao, Y., Muller, U.R., 2003. Microfluidic devices for fluidic circulation and mixing improve hybridization signal intensity on DNA arrays. Lab Chip. 3, 46–50.